Russian doll deployable meta-implants

Fusion of kirigami, origami, and multi-stability

Bobbert, F. S.L.; Janbaz, Shahram; van Manen, T.; Li, Yageng; Zadpoor, A. A.

DOI
10.1016/j.matdes.2020.108624

Publication date
2020

Document Version
Final published version

Published in
Materials and Design

Citation (APA)
Bobbert, F. S. L., Janbaz, S., van Manen, T., Li, Y., & Zadpoor, A. A. (2020). Russian doll deployable meta-implants: Fusion of kirigami, origami, and multi-stability. *Materials and Design*, *191*, Article 108624. https://doi.org/10.1016/j.matdes.2020.108624

Materials and Design 191 (2020) 108624

Contents lists available at ScienceDirect

Materials and Design

journal homepage: www.elsevier.com/locate/matdes

Russian doll deployable meta-implants: Fusion of kirigami, origami, and multi-stability

F.S.L. Bobbert *, S. Janbaz, T. van Manen, Y. Li, A.A. Zadpoor

Department of Biomechanical Engineering, Delft University of Technology, Mekelweg 2, Delft 2628CD, the Netherlands

HIGHLIGHTS

- Deployable and foldable meta-biomaterials were designed, manufactured, mechanically characterized.
- Foldable meta-biomaterials allow for the application of complex functional nanopatterns.
- Multi-layer Russian doll configurations withstand higher compression forces and offer enhanced tunability.
- A combination of origami and kirigami can be used to develop meta-implants with unusual functionalities.

GRAPHICAL ABSTRACT

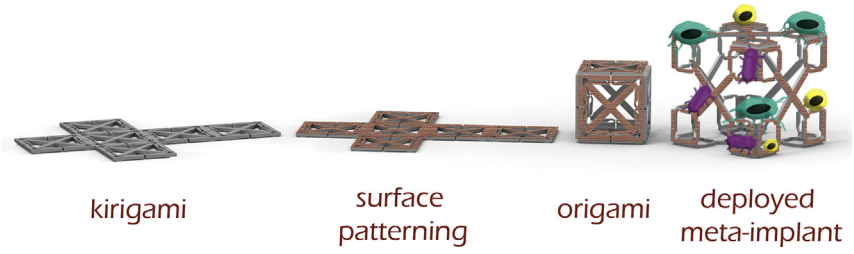

ARTICLE INFO

Article history:
Received 17 September 2019
Received in revised form 2 March 2020
Accepted 3 March 2020
Available online 05 March 2020

Keywords:
Deployable structures
Orthopaedic biomaterials
Mechanical behavior
Surface patterns

ABSTRACT

Deployable meta-implants aim to minimize the invasiveness of orthopaedic surgeries by allowing for changes in their shape and size that are triggered by an external stimulus. Multi-stability enables deployable implants to transform their shape from some compact retracted state to the deployed state where they take their full sizes and are load-bearing. We combined multiple design features to develop a new generation of deployable orthopaedic implants. Kirigami cut patterns were used to create bi-stability in flat sheets which can be folded into deployable implants using origami techniques. Inspired by Russian dolls, we designed multi-layered specimens that allow for adjusting the mechanical properties and the geometrical features of the implants through the number of the layers. Because all layers are folded from a flat state, surface-related functionalities could be applied to our deployable implants. We fabricated specimens from polylactic acid, titanium sheets, and aluminum sheets, and demonstrated that a deployment ratio of up to ≈2 is possible. We performed experiments to characterize the deployment and load-bearing behavior of the specimens and found that the above-mentioned design variables allow for adjustments in the deployment force and the maximum force before failure. Finally, we demonstrate the possibility of decorating the specimens with micropatterns.

1. Introduction

It is often said that in biological tissues such as bone, "form follows function" [1,2]. It should, thus, come as no surprise that in orthopaedic implants that replace the human bone either temporarily or permanently, 'function follows form'. This short statement summarizes the underlying principle of the so-called "meta-biomaterials" [3] and "meta-implants" [4,5], where the geometrical design at various scales is used to develop unprecedented functionalities. This novel approach, whose success depends on the feasibility of fabricating complex geometries at different scales, owes its emergence to the recent advances in additive manufacturing (AM, = 3D printing) techniques. Thanks to the "form-freedom" [6–8] and "batch-size-indifference" of AM

* Corresponding author.
E-mail address: f.s.l.bobbert@tudelft.nl (F.S.L. Bobbert).

https://doi.org/10.1016/j.matdes.2020.108624

techniques [7], the problem of developing implants with advanced functionalities reduces to the problem of geometrically designing them using the "rational design" principles [3,9].

At the microscale, the application of the rational design principles has resulted in meta-biomaterials that exhibit, for example, improved bone-implant interaction realized through the incorporation of auxetic meta-biomaterials [4] or a remarkably high level of bone-mimicry [10–12]. These uncommon properties could then be exploited to design novel meta-implants with improved bone-implant contact and, thus, enhanced longevity [4].

At the macro-scale, the fusion of geometrical design, advanced AM techniques, and rational design principles has recently enabled the development of a new category of orthopaedic implants known as "deployable implants" [5]. The shape and mechanical properties of such implants can be changed upon the application of a triggering mechanism that transforms the implant from its compact, retracted state to a fully deployed, load-bearing state. The initially compact shape of the implant ensures that the performed surgery is as minimally invasive as possible. One of the applications of such implants is to repair vertebral compression fractures. Currently, vertebroplasty (VB) and balloon kyphoplasty (BKP) are used to treat such fractures with minimal invasiveness. While VB only stabilizes the fracture by the injection of bone cement [13], BKP is a technique in which a balloon catheter is inserted and inflated prior to the injection of bone cement in order to restore the height of the vertebra [13–16]. To improve the vertebral height restoration achieved with BKP, another technique is proposed, namely vertebral body stenting (VBS) [17]. This technique uses a stent mounted on the balloon catheter that expands upon the inflation of the balloon. The expanded stent keeps the created cavity open after the balloon is removed to let the bone cement fill the cavity [13]. Although these treatments result in pain relief for the patient, cement does not allow for bony ingrowth [18]. Moreover, cement leakage as well as other complications such as persisting pain and the fracture of adjacent vertebrae may occur [19]. Our deployable implants, on the other hand, are porous devices that are deployed like the stent in VBS but do not require cement, and, thus, allow for bony ingrowth (Fig. 1a).

The underlying shape-shifting mechanism used in the design of the first generation of our deployable meta-implants [5] was the concept of "multi-stability" [20,21] where the implant is designed to have two or more stable states. By transitioning from one stable state to another, the shape and mechanical properties of the implant can change. Our first generation of deployable implants introduced the concept of deployability in orthopaedic implants and demonstrated the possibility of fabricating functional prototypes using widely available techniques. However, they were limited in two major aspects. First, they required individual printing and manual assembly of many multi-stable mechanisms. Second, due to their 3D geometry they did not allow for the incorporation of surface-related functionalities such as surface nanopatterns [22,23].

Here, we present a new generation of deployable implants that not only address those limitations but also offer some additional advantages. We used origami-based designs to fold *multi-layered* deployable implants from a flat state. The use of multiple layers is inspired by Russian dolls (Matryoshka) where identically shaped dolls that gradually increase in size successively encapsulate one another (Fig. 1b). Similar concepts can also be observed in nature (Fig. 1c). Given that each layer is folded from a flat state [24,25], advanced nanopatterning techniques that are only applicable to flat surfaces (*e.g.*, electron beam lithography [26,27], reactive ion etching (RIE) [28,29] and electron beam induced deposition [22]) could be used to simultaneously stimulate the osteogenic differentiation of stem cells [30,31] and kill bacteria [22,28].

Fig. 1. a) The novel concept of deployable implants as applied to the treatment of vertebral compression fractures. With minimally invasive surgery, a deployable structure including a balloon is placed inside the fractured vertebra. Upon the inflation of the balloon, the deployable structure expands and restores the height of the vertebra. The balloon is then removed. b) Russian dolls shown from the front and top views. c) An onion also consists of different layers. (For interpretation of the references to colour in this figure legend, the reader is referred to the web version of this article.)

2. Materials and methods

2.1. Design

We used the concept of bi-stability to design deployable flat panels. Kirigami cut patterns are known to introduce bi-stability into flat materials [32,33]. This approach to design bi-stable mechanisms is compatible with our ultimate goal of creating foldable multi-layer implants. The flat panels were then arranged in such a way to create three-dimensional cubes with varying sizes (Fig. 2f, g). Towards that end, two connection sites were designed at every corner to enable the spatial arrangement of the panels (Fig. 2a). Each panel of the unscaled (100%)

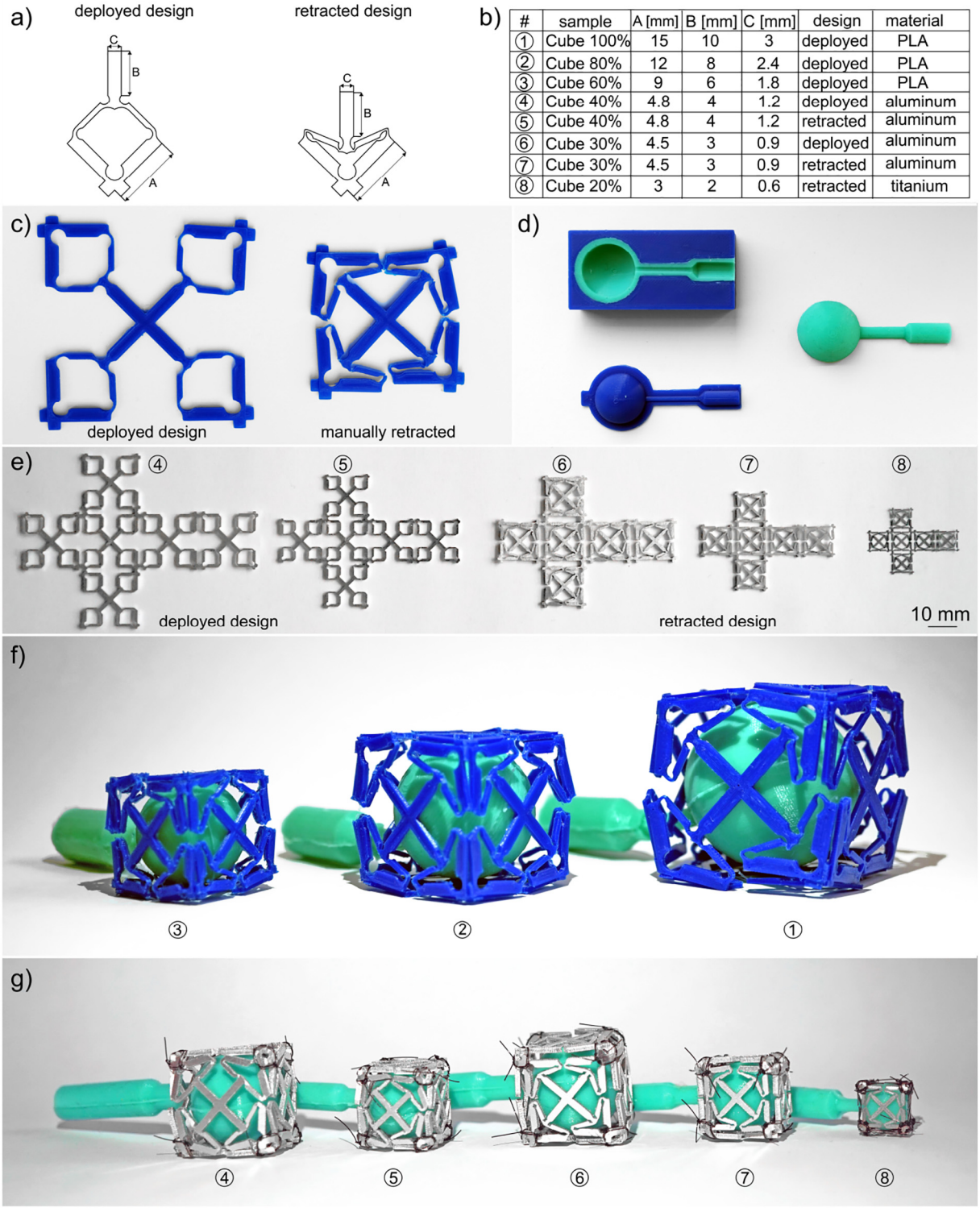

#	sample	A [mm]	B [mm]	C [mm]	design	material
①	Cube 100%	15	10	3	deployed	PLA
②	Cube 80%	12	8	2.4	deployed	PLA
③	Cube 60%	9	6	1.8	deployed	PLA
④	Cube 40%	4.8	4	1.2	deployed	aluminum
⑤	Cube 40%	4.8	4	1.2	retracted	aluminum
⑥	Cube 30%	4.5	3	0.9	deployed	aluminum
⑦	Cube 30%	4.5	3	0.9	retracted	aluminum
⑧	Cube 20%	3	2	0.6	retracted	titanium

Fig. 2. a) The parameters of the deployed and retracted designs. b) The dimensions of one corner of all specimens c) An example of a 3D printed deployed panel and a panel after manual retraction of the bi-stable elements. d) The molding of silicon balloons. e) Laser-cut aluminum specimens (scaling = 40% and 30%, both deployed and retracted conditions) and a titanium specimen (scaling = 20%, retracted). f) Balloons positioned inside the retracted control specimens. g) Balloons positioned inside the retracted origami-based specimens. From left to right: Manually retracted aluminum specimens (scaling = 40% and 30%, deployed), aluminum specimens (scaling = 40%, 30%, retracted), and a titanium specimen (scaling = 20%, retracted).

cube consisted of four bi-stable elements with two perpendicular rigid elements of 15 mm length and a rigid beam with a length of 10 mm and width of 3 mm to enable the shape transformation of the bi-stable elements (Fig. 2a).

To create the desired foldable cubes, six of the panels described above were arranged according to the unfolded shape of a cube (Fig. 2e). Two scaled versions of these unfolded states (by 30% and 40%) were also fabricated (Fig. 2b, e). In addition to the unfolded cube patterns with deployed bi-stable elements, an unfolded cube with retracted bi-stable elements was designed by cutting the deployed geometry of one deployable element at the rotation points of its hinges. The deployed element was then moved towards its retracted state (Fig. 2a). By assembling four of these elements into a rectangular panel, the unfolded pattern of a cube comprising six retracted panels was created. This cube pattern was then scaled by 20%, 30%, and 40% (Fig. 2b, e).

2.2. Manufacturing

2.2.1. PLA specimens (control group)

To evaluate the advantages of the origami approach, we fabricated similar designs using the same methodology as was used in the first generation of our deployable implants (*i.e.*, 3D printing and manual assembly). These specimens are, therefore, considered our control specimens against which the performance of our origami designs is evaluated.

The design of one panel (100%) was prepared and scaled (to 80% and 60%) in Cura (Ultimaker, The Netherlands) to prepare the files for a fused deposition modelling (FDM) 3D printer (Ultimaker 2+, Ultimaker, The Netherlands). A 0.25 mm nozzle was used to print the panels from polylactic acid (PLA) filaments. Six panels for every cube were printed. For the three different panel sizes (*i.e.*, 100%, 80%, and 60%), three different panel thicknesses were designed (*i.e.*, 2 mm, 1.5 mm, 1 mm).

2.2.2. Origami-based designs

In order to cut the specimens from metal sheets, the drawings of the unfolded cube patterns were saved as DXF files. These files were then used to laser-cut aluminum sheets (1050A) and titanium foils (purity 99.6+%, annealed; Goodfellow) with respective thicknesses of 1 mm and 0.125 mm. Three specimens of both deployed and retracted designs (scaling = 40% and 30%) were cut from aluminum sheets (12 specimens in total) using a Lion 900 laser cutter (Lion Laser Systems BV, The Netherlands). The three specimens of the retracted design (scaling = 20%) were cut from the titanium foil (3 specimens in total) using laser micromachining (Optec Laser Systems, Belgium).

2.3. Assembly of cubes

2.3.1. PLA specimens (control group)

Before the specimens with bi-stable elements were assembled, the bi-stable elements of the panels were manually brought to their retracted configurations (Fig. 2c). The specimens were then assembled by gluing the connection sites at the corners of the panels to the sides of the adjacent panels.

2.3.2. Origami-based designs

Similar to the PLA specimens, the unfolded origami specimens with a deployed design were brought to their retracted configurations. All unfolded sheets were then folded into cubes. The corners of the cubes were connected to each other with polyamide threads to hold the specimens together during the deployment process.

2.4. Balloons

Silicon balloons were manufactured in order to deploy the specimens (Fig. 2d). First, the molds were designed and printed using an FDM 3D printer (Ultimaker2+, Ultimaker, The Netherlands) and a 0.4 mm nozzle. The molds were then filled with silicon (Vinylpolysiloxane Elite Double 22, Zhermack, Italy). The inner parts of the molds were removed when the silicon was cured. Silicon was then used to connect both halves of the balloons. Since there were six different sizes of the cubes, namely control specimens (scaling = 100%, 80%, and 60%), aluminum specimens (scaling = 40% and 30%), and titanium specimens (scaling = 20%), six sizes of balloons were fabricated. The wall thickness of the balloons varied for the different sizes (2 mm for the three large balloons and 1 mm for the three smaller balloons).

The balloons were inflated using a 6 L air compressor (Michelin, France) and the required pressure was measured using the integrated pressure gauge (accuracy = 0.5 bar). The pressure was slowly increased from 0 bar to the value required to deploy the structures (Table 1).

2.5. The Russian doll (Matryoshka) principle

The Russian doll principle (Fig. 1b) was used to enhance the structural integrity of the designed deployable structures. By inserting a small cube inside a larger one, the smaller cube deploys upon the inflation of the balloon up to the point that it comes into contact with the larger one, thereby deploying it. Two versions of the Russian doll implants with two (scaling factor of the layers = 30% and 40%) and three (scaling factor of the layers = 30%, 40%, and 50%) aluminum layers were designed, laser cut, and folded (Fig. 5a,b).

2.6. Change in dimensions between the deployed and retracted structure

A caliper was used to determine the dimensions of the specimens in their retracted and deployed states. The change in the dimensions of the specimens between both configurations was determined as:

$$\text{change in dimensions } [\%] = \frac{\text{dimensions deployed structure } [\text{mm}]}{\text{dimensions retracted structure } [\text{mm}]} \times 100.$$

2.7. Compression tests

The mechanical properties of the different designs were determined using compression tests. Before the mechanical tests were performed, the balloons were removed from the deployed structures. The specimens were uniaxially compressed using a Lloyd LR5K mechanical testing machine at a crosshead velocity of 1 mm/min. Two load cells (5 kN and 100 N) were used depending on the expected range of the forces to compress the control specimens and the aluminum specimens. In the case of the single-layer specimens, the tests were aborted when either a 50 N force was reached or when the specimens were compressed to 60% of their deployed size. For the Russian doll specimens, the specimens were allowed to experience higher forces. For the compression of the titanium structures, a velocity of 0.5 mm/min and a 5 N load cell were used. These tests were aborted when a maximum force of 4.95 N was reached to prevent damage to the load cell. In order to evaluate the effects of friction at the interface of the compression plates and the control specimens, sandpaper (P80) was used for the compression of the control specimens (scaling = 80%) (*i.e.* PLA cubes) with a thickness of 1.5 mm. These specimens were chosen because they were the least fragile during the manual retraction of the bi-stable elements and the deployment of the specimens.

Table 1
The dimensions of the retracted and deployed specimens with their thickness, volume change, and the type of the material. The numbers between round brackets indicate the number of the intact specimens and the number followed by ~ is the number of the specimens with fractured parts. Example: (1 + 2~) means that the dimensions were measured from one intact specimen and two specimens with fractures.

	Dimensions of configuration [mm]		Thickness [mm]	Change in dimensions [%]	Material	Maximum pressure [bar]
	Retracted	Deployed				
Cube 100% deployed	37.8 ± 0.5	46.1 ± 1.9	1	124 ± 7.5 (4~)	PLA	≈0.1
	37.2 ± 0.6	48.7 ± 1.7	1.5	131 ± 9.0 (2 + 1~)	PLA	≈0.1
	38.2 ± 0.3	51 ± 1.5	2	133 ± 5.6 (4~)	PLA	≈0.1
Cube 80% deployed	30.6 ± 0.3	37.1 ± 0.7	1	121 ± 3.5 (3 + 1~)	PLA	≈0.2
	31.2 ± 0.2	39.9 ± 0.6	1.5	128 ± 2.3 (3)	PLA	≈0.2
	31.0 ± 0.3	40.5 ± 0.3	2	130 ± 1.5 (1 + 1~)	PLA	≈0.2
Cube 60% deployed	23.5 ± 0.2	30.8 ± 1.0	1	129 ± 4.6 (3 + 1~)	PLA	≈0.5
	24.1 ± 0.4	30.4 ± 0.2	1.5	124 ± 4.4 (1 + 1~)	PLA	≈0.5
	24.7 ± 0.1	29.8 ± 0.3	2	119 ± 4.5 (2)	PLA	≈0.5
Cube 40% deployed	17.5 ± 0.1	28 ± 0.3	1	164 ± 7.6 (3)	Aluminum	≈1.5
Cube 30% deployed	13.5 ± 0.1	22.4 ± 1.1	1	166 ± 9.0 (3)	Aluminum	≈2
Cube 40% retracted	17.0 ± 0.1	29.5 ± 1.2	1	173 ± 6.1 (3)	Aluminum	≈1.2
Cube 30% retracted	13.2 ± 0.2	20.8 ± 0.2	1	158 ± 7.5 (3)	Aluminum	≈1.4
Cube 20% retracted	7.7 ± 0.1	13.8 ± 0.5	0.125	179 ± 7.2 (3)	Titanium	≈1.5
Russian doll specimen, two layers	17.0 ± 0.3	26.7 ± 1.7	2	157 ± 10.8 (3~)	Aluminum	≈2.5
Russian doll specimen, three layers	20.5 ± 0.1	27.1 ± 0.5	3	132 ± 2.7 (1 + 2~)	Aluminum	≈3.5

2.8. Micropatterns

Micropatterns were created on titanium foil to demonstrate the concept of patterning a flat sheet that can be folded afterwards. The patterns included circles and squares with a diameter and edge lengths of 65 μm, respectively. The wavy pattern consisted of waves with a length of 5 mm and an amplitude of 0.25 mm. These micropatterns were engraved into a titanium foil through laser micromachining (Optec Laser Systems, Belgium). To engrave the sheet, the laser frequency (50 kHz) and current (3.8 A) were kept constant, while the firing rate (30 kHz, 50 kHz and 70 kHz) and the number of repetitions ($n = 2$, $n = 10$, $n = 20$, $n = 30$, $n = 40$) were varied. After engraving, the specimen was cleaned with demineralized water and detergent in an ultrasonic bath for 10 min followed by rinsing with demineralized water in the ultrasonic bath for another 5 min. A Keyence VH-Z250R (Keyence, Japan) digital microscope was used to determine the depth, diameter, and width of the micropatterns.

3. Results

3.1. Inflation of balloons and mechanical tests

3.1.1. PLA specimens (control group)

The deployment of a cube was considered successful when it deployed without any fractures. Out of a total of 43 control specimens (*i.e.*, PLA cubes), 16 cubes were successfully deployed. Some of the partially damaged cubes were still measurable with either one fracture (7 cubes), two fractures (2 cubes), or with more than two fractures (2 cubes). For the control specimens that fractured during inflation, one replacement cube was manufactured in order to be able to test more than one specimen under compression. For the control specimens (scaling = 60%) with a thickness of 1.5 mm, three replacement cubes were made of which only one could be used for the compression tests. The control specimens (scaling = 80%) with a thickness of 1.5 mm were all successfully deployed (Fig. 3a).

The smallest change in the dimensions was observed for the control specimens (scaling = 60%) with a thickness of 2 mm. The maximum pressure required to deploy the different control specimens varied between 0.1 and 0.5 bar. The control specimens (scaling = 60%) required the highest pressure while the unscaled control specimens (100% cube) required the lowest pressure (Table 1).

3.1.2. Origami-based designs

All origami-based specimens with a single layer were successfully deployed (Fig. 4a). Signs of fractures were only observed in the smallest cube of the multi-layer Russian doll specimens. As expected, the smallest cube was deployed first until it was in contact with the medium-sized cube. Upon further inflation of the balloon, both cubes deployed together until deployment was restricted by the maximum deployment of the smallest cube. To complete the deployment of the third cube, we needed to use another balloon to continue the inflation process. When comparing the changes in the configuration between the different specimens, the origami-based designs showed a larger change in the dimensions as compared to the control group (Table 1). The titanium specimens showed the best results with a change of 179% (Table 1).

The aluminum specimens (scaling = 30% and 40%) required ≈1.2–2 bar to deploy. The more complex Russian doll specimens with two or three layers of cubes required a higher pressure than all other specimens (Table 1). The Russian doll specimens with three layers could not be deployed with a single balloon due to the rupture of the balloon at ≈3.5 bar. A larger balloon to inflate the origami-based specimens (scaling = 40%) was inserted and could deploy the last part of the specimen. The titanium specimens could be deployed with a pressure of ≈1.5 bar.

3.2. Compression tests

3.2.1. PLA specimens (control group)

The control specimens which included less than three fractures after inflation were compressed with 1 mm/min using a Lloyd LR5K testing machine. During the tests, the deployable elements slowly retracted (Fig. 3b). As expected, the cubes with thicker planes required more force to be compressed (Fig. 3d). The force-displacement curves of the specimens that neatly retracted without out-of-plane deformations showed a steep slope at their end phases (Fig. 3d). The curves of the specimens with a thickness of 1 mm were relatively smooth as compared to those of thicker specimens (Fig. 3d).

When sandpaper was applied to the top and bottom of the control specimens (scaling = 80%) with a thickness of 1.5 mm, no retraction of the panels at the top and bottom was observed (Fig. 3c). However, fracture and out-of-plane deformation of the vertical panels were observed (Fig. 3c). The force-displacement graph shows that the same force is required to deform the control specimens (scaling =

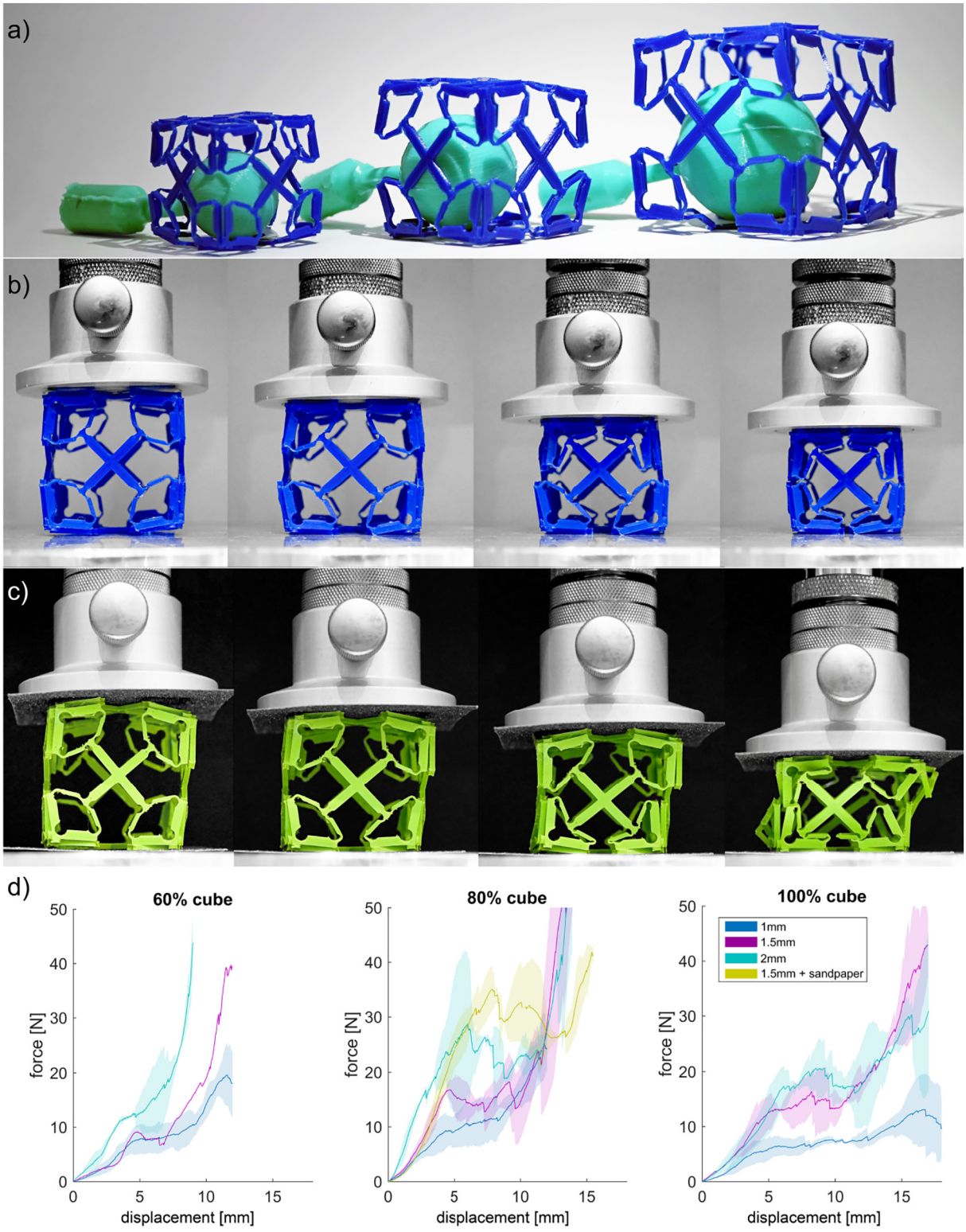

Fig. 3. PLA specimens (control group). a) Deployed control specimens (scaling = 60%, 80%, 100%). b) The compressive behavior of a control specimen (scaling = 80%, thickness = 1.5 mm). c) The compressive behavior of a control specimen with sandpaper (scaling = 80%, thickness = 1.5 mm). d) The force-displacement curves of the control specimens (scaling = 60%, 80%, and 100%).

80%) with a thickness of 1.5 mm with and without sandpaper up to 4 mm (Fig. 3d). The difference is visible after this point, where the force still increases for a specimen with sandpaper and slightly decreases for the same specimen compressed without sandpaper (Fig. 3d).

3.2.2. Origami-based designs

All single-layer specimens developed a spherical shape thanks to the forces transmitted from the balloon to the cubic specimens (Fig. 4a). The multi-layer Russian doll specimens also developed a spherical shape, although to a lesser extent than the single-layer specimens (Fig. 5c).

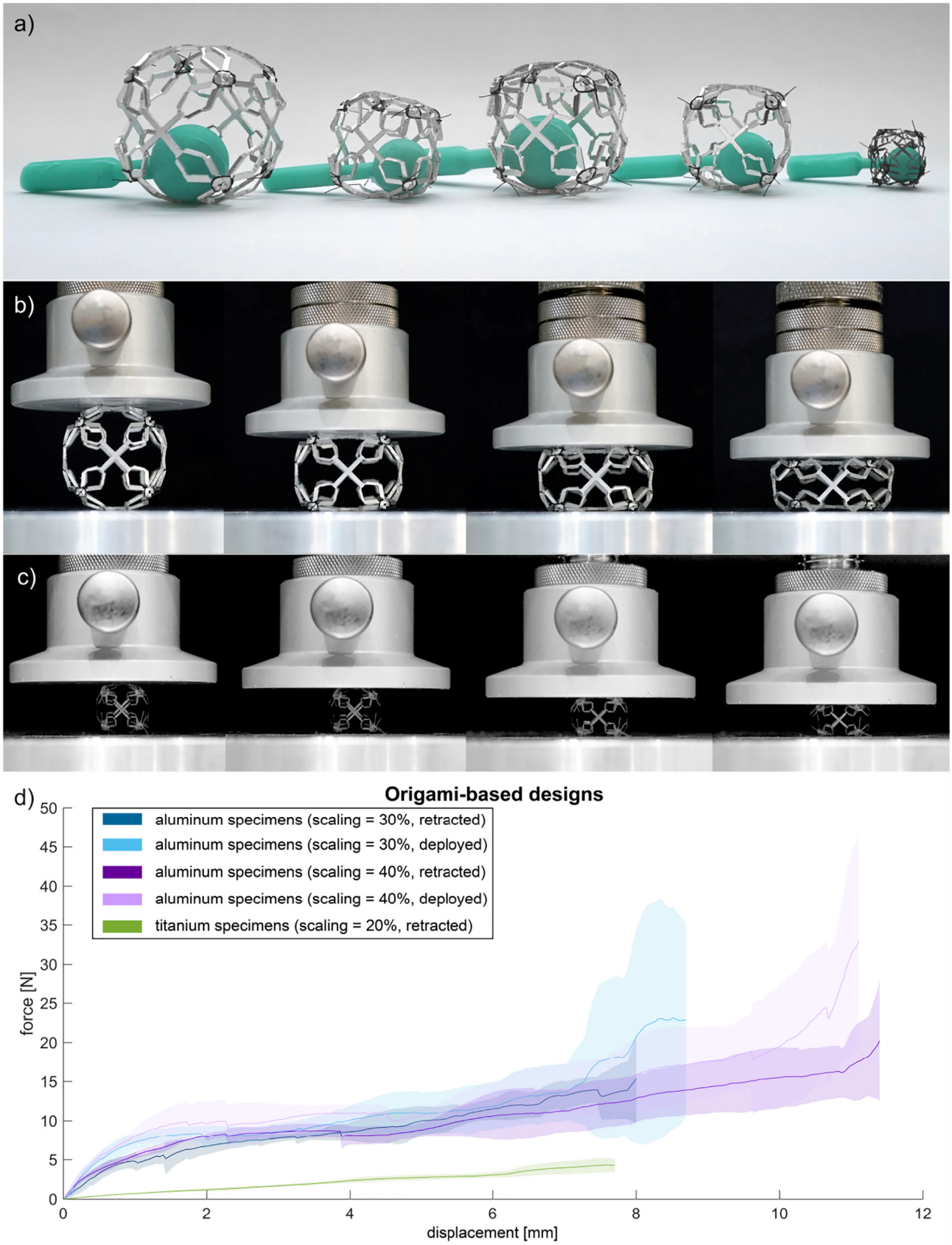

Fig. 4. Origami-based design. a) Deployed origami-based specimens. Two deployed aluminum specimens (scaling = 40% and 30%), two retracted aluminum specimens (scaling = 40% and 30%), and a retracted titanium specimen (scaling = 20%). b) The compression of an aluminum specimen. c) The compression of a titanium specimen. d) The force-displacement curves of the origami-based specimens.

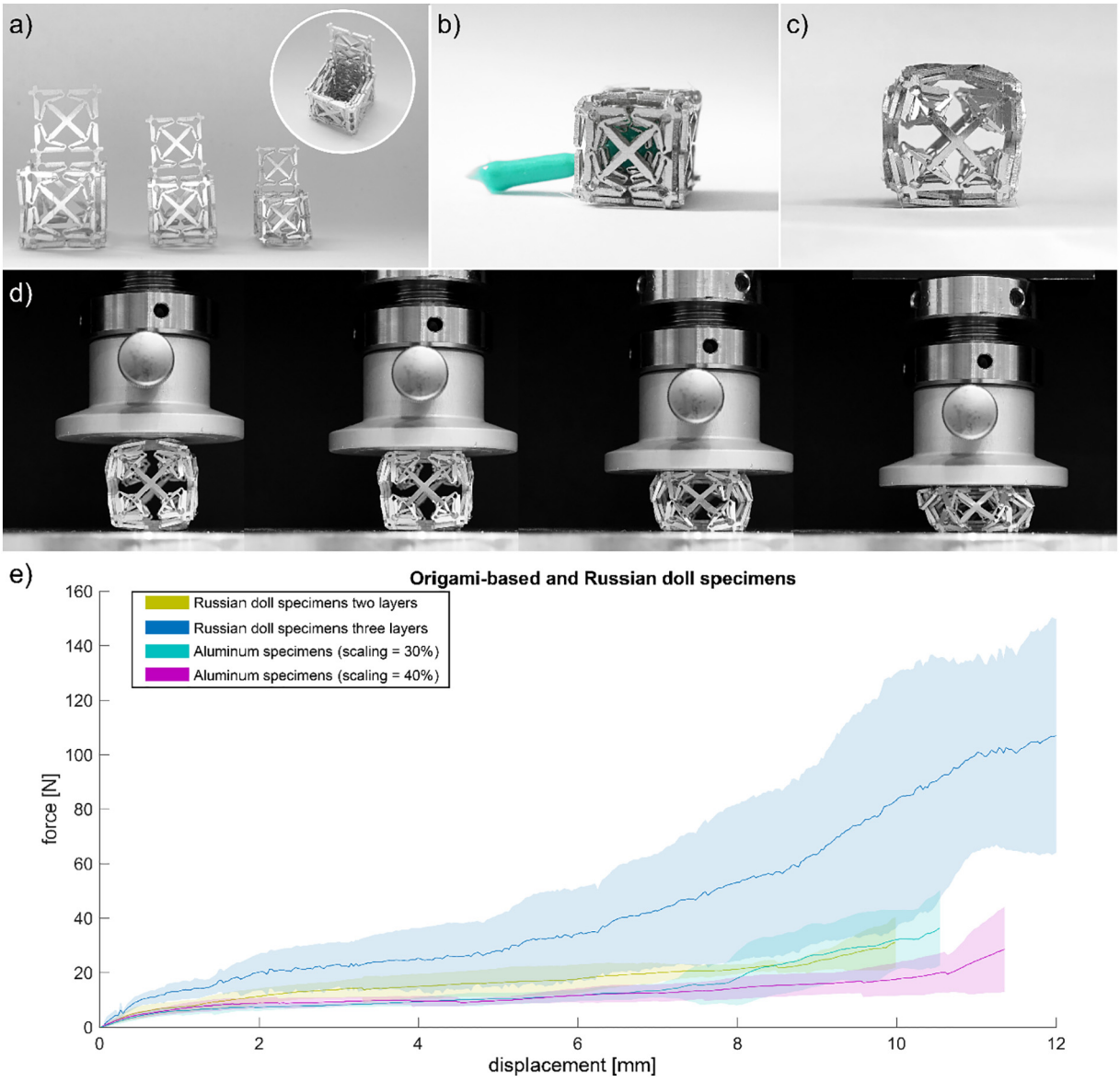

Fig. 5. The Russian doll principle. a) Three aluminum cubes are shown from the front view and a top view of a small cube within two larger cubes. b) Retracted Russian doll specimens with three layers (scaling factor of the layers = 30%, 40%, and 50%, aluminum). c) A multi-layer Russian doll specimen with three layers shown after deployment. d) The compression of a Russian doll specimen with three layers. e) The force-displacement curves of the Russian doll specimens and the aluminum single-layer specimens (scaling = 30%, 40%).

While one of the three multi-layer specimens deployed fully symmetrically, the outer layer of the two other specimens contained one or two retracted planes. As opposed to the control specimens, the origami-based specimens did not return to their retracted configuration during the compression tests. Instead, they flattened into disc-like shapes without retracted elements (Fig. 4b, c). For the 30% and 40% specimens, initially more force was required to compress these specimens as compared to their retracted counterparts (Fig. 4d). For all origami-based specimens, initially a higher compression force was required to deform the specimens as compared to the control specimens (Figs. 3d, 4d).

The titanium specimens showed the least variation in the measured forces and required the least amount of force to be compressed (Fig. 4d).

When comparing the force-displacement curves of the two-layer Russian doll specimens (Fig. 5) with those of the single-layer aluminum (scaling = 30% and 40%) specimens, we found that their initial stiffness is comparable up to 1 mm of displacement (Fig. 5e). However, after this point, more force is required to compress the Russian doll specimens, as compared to the single-layer specimens (Fig. 5e). The three-layer Russian doll specimens required the most compression force of all specimens in this study (Fig. 5e).

3.3. Micropatterns

The designed micropatterns were successfully engraved onto the surface of the titanium foil (Fig. 6, top inset). By keeping the frequency and current of the laser constant but varying the firing rates and the number of repetitions, different depths and quality of the shapes could be achieved. The squares and circles engraved with a firing rate of 70 kHz and 10 repetitions yielded in the most accurate micropatterns in terms of their similarity to the designs. The depth of the patterns depended on the combinations of firing rate and the number of repetitions. A higher number of repetitions resulted in a deeper engraving on the titanium foil. The depth of the micropatterns varied between 2 μm for the wave pattern to 60 μm for the circles.

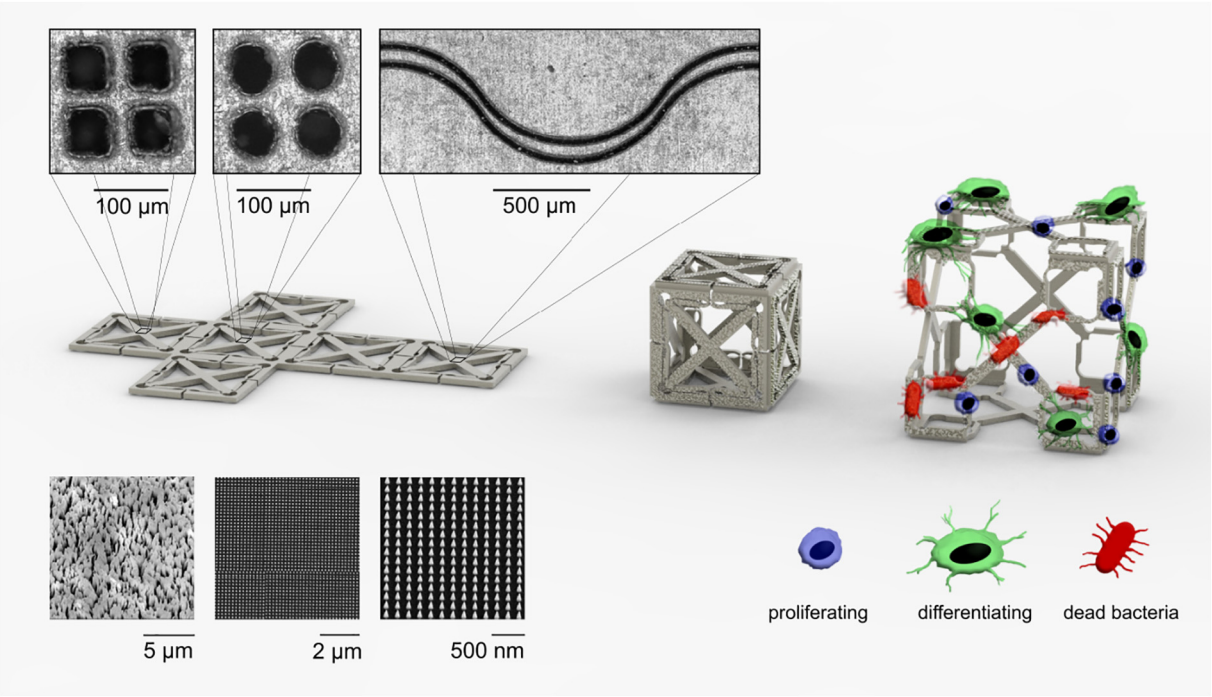

Fig. 6. The concept of surface micropatterns and nanopatterns as applied to deployable meta-implants. Top inset: three micropatterns were engraved into a titanium sheet metal specimen (squares, circles and waves). Bottom inset: Some examples of different nanopatterns with specific features (*e.g.*, bactericidal, osteogenic) that could be applied to flat sheets. Left: nanostructures created using RIE, fabrication described by Ganjian et al. [29], center and right: nanopillars created using EBID [22]. After applying the nanopatterns, the flat specimen can be folded and deployed as meta-implants with different surface-related functionalities.

4. Discussion

We showed, for the first time ever, how the principles of multi-stability, kirigami, and origami could be combined to create deployable meta-implants with precisely controlled and arbitrarily complex surface patterns. The deployment of the designed meta-implants can be easily performed using inflating balloons. A similar balloon-based inflation procedure is already applied as a part of a procedure used to treat vertebral compression fractures minimally invasively, namely balloon kyphoplasty (BKP). Our designs could provide a potential replacement for the stents used in vertebral body stenting (VBS) [34–36], which is a proposed alternative for BKP. This shows the feasibility of our approach and could facilitate the clinical adoption of such implants.

4.1. Deployability

The results of our study clearly show the superior performance of origami-based designs over the control specimens, which were designed and manufactured using the principles introduced in our previous generation of deployable meta-implants. This superior performance is clear in terms of the successful deployment of the meta-implant specimens, the ease of manufacturing, the possibility to incorporate surface nanopatterns and other surface related bio-functionalities, and the mechanical properties.

The design and fabrication of basic elements that exhibit a reliable bi-stable behavior is one of the major challenges in the design of deployable meta-implants. In this study, the use of kirigami as the mechanism through which bi-stability was created enabled us to fold the meta-implants from a flat state using origami principles. This is one of the areas of application where both kirigami and origami principles are required and each plays a different role.

In terms of the deployment ratio, the origami-based designs achieved up to ≈2 times larger dimensions after deployment. Given the fact that the volume of the implant has a cubic relationship with the dimensions of the specimens, a two-fold increase in dimensions translates into an eight-fold decrease in the initial volume of the implant and, thus, drastically reduces the invasiveness of the surgery. The design and dimensions of the kirigami cut patterns could be used to adjust the deployment ratio. Studying the design of the kirigami patterns is, therefore, a systematic way for the study of the multi-stable behavior of the implants and provides a general design platform within which deployable meta-implants could be "rationally designed" using predictive computational models.

The origami-based specimens developed a sphere-like shape after deployment. This was due to the fact that the balloon used for their deployment was spherical. Such a rounded shape may be desirable in cases where the sharp edges of the cubic specimens are not compatible with the anatomical shapes that are being operated on. It is, of course, also possible to chamfer the cubic specimens at the design stage.

This change in the shape of the implant after deployment goes far beyond the above-mentioned rounding effect and showcases an interesting and important property of our origami-based meta-implants, namely their shape-morphing behavior. In practice, there are also external boundaries (*i.e.*, bony contours) that define the ultimate shape of the deployed meta-implant. The origami-based designs could, therefore, match the shape of their external boundaries. This eliminates the need for designing implants that match a specific (patient-specific) shape and enables us to use the same (generic) implant for different patients.

4.2. Mechanical performance

There are several novel design features in the work presented here that could be used to address the structural challenges faced when designing deployable meta-implants. The Russian doll concept is a particularly interesting approach, because it allows for a high level of adjustability in terms of the mechanical properties of the meta-implant as well as its dimensions. Each additional layer results in a multi-fold increase in the force corresponding to the same displacement (Fig. 5). Simply adding an additional layer could, therefore, be used to reinforce the implant further for the cases where higher forces are

expected (*e.g.*, adult, obese patients) while a smaller number of layers could be used in other cases (*e.g.*, pediatric patients) to be able to strike a balance between the requirement to provide enough structural performance and the risk of causing stress shielding. The porous structure of the implant also allows for other types of reinforcing mechanisms to be used for improving the mechanical properties of the meta-implants further. For example, deploying wire-like objects that coil within a confined space (similar to [37]) could drastically increase the mechanical properties of the implant. Furthermore, given the fact that porous structures allow for bony ingrowth, the mechanical properties of the implant are expected to gradually increase with the progress of the bone tissue regeneration. A previous study has shown that the quasi-static and fatigue mechanical properties of porous structures could increase by up to 7 fold upon bony ingrowth [38]. Moreover, the choice of the material could be used to further increase the mechanical properties of the implant. In this study, we used sheets that were made from pure titanium and aluminum, which are highly deformable but whose mechanical properties are several times lower than other titanium alloys that could be used for the fabrication of orthopaedic implants (*e.g.*, Ti-6Al-4 V). Finally, the sheet thickness could be used to adjust the mechanical properties of the meta-implants. It is, however, worth noting that the bendability of metal sheets decreases with the thickness. In summary, there are several design strategies that allow for the adjustment of the mechanical properties of the meta-implants developed here and could be used in the future studies to tailor the mechanical properties of deployable implants to the specific problem at hand. Many aspects of such types of implants including their behavior under dynamic loading conditions also need to be studied before they could be used in clinical practice.

4.3. Surface nanopatterns and other bio-functionalities

The fact that our origami-based designs are folded from a flat state makes it possible to use surface nanopatterning techniques that usually only work on flat surfaces [39]. We used laser micromachining to create some micropatterns on the titanium foil that was also used for our deployable meta-implants. It is, however, possible to use virtually any type of micro-/nanopatterning technique including the ones we have applied in our other studies to titanium and other biomedically relevant materials (Fig. 6). With techniques such as electron beam induced deposition (EBID, a nanoscale 3D printing technique) [22,22], electron beam nanolithography [26,27], and reactive ion etching (RIE) [28,40], it is possible to create precisely-controlled and arbitrarily complex surface nanopatterns at scales ranging between a few nanometers (in the case of EBID) to hundreds of nanometers (nanolithography, RIE).

A growing body of recent research shows that surface nanopatterns could be used to both determine stem cell fate [41–43] and prevent implant-associated infections [27,22]. In both cases, the primary action mechanism is mechanical in nature. Regarding the stem cell fate, surface nanopatterns result in cytoskeletal re-arrangement, regulate focal adhesions, and may upregulate the expression of osteogenic markers [44]. This kind of mechanobiological pathways does not require any pharmaceutical agent, meaning that it is less expensive and safer to implement in clinical practice. Moreover, the certification of medical devices that do not incorporate pharmaceutics is more streamlined as compared to those that incorporate one or more active agents.

In the case of bacteria, a mechanical mechanism where the asperities of the nanopattern strain the cell wall of bacteria and cause them to rupture is often cited as the mechanism through which surface nanopatterns kill bacteria [27,22,45]. Similar to the case of stem cells, this is a drugless approach whose success is not dependent on the potency of any specific drug, making it easier for medical devices to be certified for clinical use. Even more importantly, antibiotic resistance is not a problem in the case of surface nanopatterns, meaning that even multi-drug resistant bacteria could be killed using this approach.

It is important to realize that the bio-functionality of the deployable meta-implants presented here is also dependent on the design of the kirigami cut patterns, the thickness of the metal sheets used for creating the different layers of the implants, and the number of the layers in the Russian doll designs. That is because these design choices determine the geometrical parameters of such a porous implant including the porosity and pore size. Given the fact that bone tissue regeneration is highly dependent on such geometrical parameters [46,47], the geometrical design of deployable meta-implants could potentially affect their ultimate bone tissue regeneration performance. This and many other aspects of deployable meta-implants need to be studied in future studies.

5. Conclusions

We designed and fabricated a new generation of deployable meta-implants using a combination of origami, kirigami, and multi-stability principles. We also applied a multi-layer design, which was inspired by Russian dolls and is also observed in nature. The design strategies applied in the study allow for systematic adjustments of the deployment force, deployment ratio, mechanical properties, pore size, and porosity of the resulting meta-implants. The specimens were manufactured from a variety of materials including PLA, aluminum, and titanium. We also characterized the deployment behavior and mechanical properties of the manufactured specimens. Since the fabrication of origami-based implants starts from a flat state, it is possible to incorporate precisely-controlled and arbitrarily complex surface micro-/nanopatterns onto the specimens. We demonstrated the feasibility of such surface bio-functionalization using laser micromachining. The various functionalities of our design including their deployability, the tunability of the dimensions and mechanical properties, and the applicability of complex surface patterns make these structures a potential replacement for the stents used in vertebral body stenting. The combination of their high porosity and surface nanopatterns could be used to promote bone regeneration and eliminate the use of bone cement. Future studies are suggested for taking further steps that are required for the clinical adoption of the presented designs. The techniques used in the current study are relatively inexpensive in their nature. However, the use of manual labor should be replaced by mass production procedures. Since the proposed approach is amenable to the implementation of these techniques, the production costs of the deployable implants are not expected to be excessively high.

CRediT authorship contribution statement

F.S.L. Bobbert: Conceptualization, Methodology, Validation, Investigation, Writing - original draft, Visualization. **S. Janbaz:** Methodology, Writing - review & editing. **T. van Manen:** Methodology, Writing - review & editing. **Y. Li:** Methodology, Writing - review & editing. **A.A. Zadpoor:** Writing - review & editing, Supervision.

Declaration of competing interest

The authors declare that they have no known competing financial interests or personal relationships that could have appeared to influence the work reported in this paper.

Acknowledgements

The research leading to these results has received funding from the European Research Council under the ERC grant agreement no. [677575].

References

[1] D. Sommerfeldt, C. Rubin, Biology of bone and how it orchestrates the form and function of the skeleton, Eur. Spine J. 10 (2) (2001) S86–S95.

[2] E.F. Morgan, G.L. Barnes, T.A. Einhorn, The bone organ system: form and function, Osteoporosis, Elsevier (2013) 3–20.
[3] A.A. Zadpoor, Mechanical performance of additively manufactured meta-biomaterials, Acta Biomater. 85 (2019) 41–59.
[4] H.M. Kolken, S. Janbaz, S.M. Leeflang, K. Lietaert, H.H. Weinans, A.A. Zadpoor, Rationally designed meta-implants: a combination of auxetic and conventional meta-biomaterials, Mater. Horiz. 5 (1) (2018) 28–35.
[5] F. Bobbert, S. Janbaz, A. Zadpoor, Towards deployable meta-implants, J. Mater. Chem. B 6 (2018) 3449–3455.
[6] S.A. Tofail, E.P. Koumoulos, A. Bandyopadhyay, S. Bose, L. O'Donoghue, C. Charitidis, Additive manufacturing: scientific and technological challenges, market uptake and opportunities, Mater. Today 21 (1) (2018) 22–37.
[7] A. Zadpoor, Design for additive bio-manufacturing: from patient-specific medical devices to rationally designed meta-biomaterials, Int. J. Mol. Sci. 18 (8) (2017) 1607.
[8] A. Yánez, A. Cuadrado, O. Martel, H. Afonso, D. Monopoli, Gyroid porous titanium structures: a versatile solution to be used as scaffolds in bone defect reconstruction, Mater. Des. 140 (2018) 21–29.
[9] O. Bas, S. Lucarotti, D.D. Angella, N.J. Castro, C. Meinert, F.M. Wunner, E. Rank, G. Vozzi, T.J. Klein, I. Catelas, Rational design and fabrication of multiphasic soft network composites for tissue engineering articular cartilage: a numerical model-based approach, Chem. Eng. J. 340 (2018) 15–23.
[10] S.-I. Roohani-Esfahani, P. Newman, H. Zreiqat, Design and fabrication of 3D printed scaffolds with a mechanical strength comparable to cortical bone to repair large bone defects, Sci. Rep. 6 (2016), 19468.
[11] S. Arabnejad, R.B. Johnston, J.A. Pura, B. Singh, M. Tanzer, D. Pasini, High-strength porous biomaterials for bone replacement: a strategy to assess the interplay between cell morphology, mechanical properties, bone ingrowth and manufacturing constraints, Acta Biomater. 30 (2016) 345–356.
[12] P. Ouyang, H. Dong, X. He, X. Cai, Y. Wang, J. Li, H. Li, Z. Jin, Hydromechanical mechanism behind the effect of pore size of porous titanium scaffolds on osteoblast response and bone ingrowth, Mater. Des. 183 (2019), 108151.
[13] P. Diel, C. Röder, G. Perler, T. Vordemvenne, M. Scholz, F. Kandziora, S. Fürderer, S. Eiskjaer, G. Maestretti, R. Rotter, Radiographic and safety details of vertebral body stenting: results from a multicenter chart review, BMC Musculoskelet. Disord. 14 (1) (2013) 233.
[14] I. Lieberman, S. Dudeney, M.-K. Reinhardt, G. Bell, Initial outcome and efficacy of "kyphoplasty" in the treatment of painful osteoporotic vertebral compression fractures, spine 26 (14) (2001) 1631–1637.
[15] D.R. Fourney, D.F. Schomer, R. Nader, J. Chlan-Fourney, D. Suki, K. Ahrar, L.D. Rhines, Z.L. Gokaslan, Percutaneous vertebroplasty and kyphoplasty for painful vertebral body fractures in cancer patients, J. Neurosurg. Spine 98 (1) (2003) 21–30.
[16] F.M. Phillips, F.T. Wetzel, I. Lieberman, M. Campbell-Hupp, An in vivo comparison of the potential for extravertebral cement leak after vertebroplasty and kyphoplasty, Spine 27 (19) (2002) 2173–2178.
[17] S. Fürderer, M. Anders, B. Schwindling, M. Salick, C. Düber, K. Wenda, R. Urban, M. Glück, P. Eysel, Vertebral body stenting, Orthopade 31 (4) (2002) 356–361.
[18] I.H. Lieberman, D. Togawa, M.M. Kayanja, Vertebroplasty and kyphoplasty: filler materials, Spine J. 5 (6) (2005) S305–S316.
[19] A. Krueger, C. Bliemel, R. Zettl, S. Ruchholtz, Management of pulmonary cement embolism after percutaneous vertebroplasty and kyphoplasty: a systematic review of the literature, Eur. Spine J. 18 (9) (2009) 1257–1265.
[20] X. Lachenal, P.M. Weaver, S. Daynes, Multi-stable composite twisting structure for morphing applications, Proceedings of the Royal Society A: Mathematical, Physical and Engineering Sciences 468 (2141) (2012) 1230–1251.
[21] S. Shan, S.H. Kang, J.R. Raney, P. Wang, L. Fang, F. Candido, J.A. Lewis, K. Bertoldi, Multistable architected materials for trapping elastic strain energy, Adv. Mater. 27 (29) (2015) 4296–4301.
[22] M. Ganjian, K. Modaresifar, M.R. Ligeon, L.B. Kunkels, N. Tümer, L. Angeloni, C.W. Hagen, L.G. Otten, P.L. Hagedoorn, I. Apachitei, Nature helps: toward bioinspired bactericidal nanopatterns, Adv. Mater. Interfaces 6 (16) (2019) 1900640.
[23] K.S. Brammer, S. Oh, C.J. Cobb, L.M. Bjursten, H. van der Heyde, S. Jin, Improved bone-forming functionality on diameter-controlled TiO2 nanotube surface, Acta Biomater. 5 (8) (2009) 3215–3223.
[24] S.J. Callens, N. Tümer, A.A. Zadpoor, Hyperbolic origami-inspired folding of triply periodic minimal surface structures, Appl. Mater. Today 15 (2019) 453–461.
[25] S. Janbaz, N. Noordzij, D.S. Widyaratih, C.W. Hagen, L.E. Fratila-Apachitei, A.A. Zadpoor, Origami lattices with free-form surface ornaments, Sci. Adv. 3 (11) (2017) eaao1595.
[26] C. Vieu, F. Carcenac, A. Pepin, Y. Chen, M. Mejias, A. Lebib, L. Manin-Ferlazzo, L. Couraud, H. Launois, Electron beam lithography: resolution limits and applications, Appl. Surf. Sci. 164 (1–4) (2000) 111–117.
[27] H. Shahali, J. Hasan, A. Mathews, H. Wang, C. Yan, T. Tesfamichael, P.K. Yarlagadda, Multi-biofunctional properties of three species of cicada wings and biomimetic fabrication of nanopatterned titanium pillars, J. Mater. Chem. B 7 (8) (2019) 1300–1310.
[28] J. Hasan, S. Jain, K. Chatterjee, Nanoscale topography on black titanium imparts multi-biofunctional properties for orthopedic applications, Sci. Rep. 7 (1) (2017) 1–13.
[29] M. Ganjian, K. Modaresifar, H. Zhang, P.-L. Hagedoorn, L.E. Fratila-Apachitei, A.A. Zadpoor, Reactive ion etching for fabrication of biofunctional titanium nanostructures, Sci. Rep. 9 (1) (2019) 1–20.
[30] K. Ye, X. Wang, L. Cao, S. Li, Z. Li, L. Yu, J. Ding, Matrix stiffness and nanoscale spatial organization of cell-adhesive ligands direct stem cell fate, Nano Lett. 15 (7) (2015) 4720–4729.
[31] P. Tsimbouri, L. Fisher, N. Holloway, T. Sjostrom, A. Nobbs, R.D. Meek, B. Su, M. Dalby, Osteogenic and bactericidal surfaces from hydrothermal titania nanowires on titanium substrates, Sci. Rep. 6 (2016), 36857.
[32] X. Shang, L. Liu, A. Rafsanjani, D. Pasini, Durable bistable auxetics made of rigid solids, J. Mater. Res. (2017) 1–9.
[33] T.C. Shyu, P.F. Damasceno, P.M. Dodd, A. Lamoureux, L. Xu, M. Shlian, M. Shtein, S.C. Glotzer, N.A. Kotov, A kirigami approach to engineering elasticity in nanocomposites through patterned defects, Nat. Mater. 14 (8) (2015) 785.
[34] D. Vanni, A. Pantalone, F. Bigossi, F. Pineto, D. Lucantoni, V. Salini, New perspective for third generation percutaneous vertebral augmentation procedures: preliminary results at 12 months, Journal of Craniovertebral Junction and Spine 3 (2) (2012) 47.
[35] J. Garnon, B. Doré, P. Auloge, J. Caudrelier, D. Dalili, N. Ramamurthy, G. Koch, R.L. Cazzato, A. Gangi, Efficacy of the vertebral body stenting system for the restoration of vertebral height in acute traumatic compression fractures in a non-osteoporotic population, Cardiovasc. Intervent. Radiol. 42 (11) (2019) 1579–1587.
[36] S. Schützenberger, S. Schwarz, L. Greiner, O. Holub, S. Grabner, W. Huf, A. Sailler, C. Fialka, Is vertebral body stenting in combination with CaP cement superior to kyphoplasty? Eur. Spine J. 27 (10) (2018) 2602–2608.
[37] M.R. Shaebani, J. Najafi, A. Farnudi, D. Bonn, M. Habibi, Compaction of quasi-one-dimensional elastoplastic materials, Nat. Commun. 8 (2017), 15568.
[38] R. Hedayati, S. Janbaz, M. Sadighi, M. Mohammadi-Aghdam, A. Zadpoor, How does tissue regeneration influence the mechanical behavior of additively manufactured porous biomaterials? J. Mech. Behav. Biomed. Mater. 65 (2017) 831–841.
[39] Y. Liu, J. Genzer, M.D. Dickey, "2D or not 2D": shape-programming polymer sheets, Prog. Polym. Sci. 52 (2016) 79–106.
[40] T.U. Luu, S.C. Gott, B.W. Woo, M.P. Rao, W.F. Liu, Micro-and nanopatterned topographical cues for regulating macrophage cell shape and phenotype, ACS Appl. Mater. Interfaces 7 (51) (2015) 28665–28672.
[41] L. Bacakova, E. Filova, M. Parizek, T. Ruml, V. Svorcik, Modulation of cell adhesion, proliferation and differentiation on materials designed for body implants, Biotechnol. Adv. 29 (6) (2011) 739–767.
[42] T. Gong, J. Xie, J. Liao, T. Zhang, S. Lin, Y. Lin, Nanomaterials and bone regeneration, Bone Res. 3 (2015), 15029.
[43] T. Sjöström, M.J. Dalby, A. Hart, R. Tare, R.O. Oreffo, B. Su, Fabrication of pillar-like titania nanostructures on titanium and their interactions with human skeletal stem cells, Acta Biomater. 5 (5) (2009) 1433–1441.
[44] E.K. Yim, E.M. Darling, K. Kulangara, F. Guilak, K.W. Leong, Nanotopography-induced changes in focal adhesions, cytoskeletal organization, and mechanical properties of human mesenchymal stem cells, Biomaterials 31 (6) (2010) 1299–1306.
[45] E.P. Ivanova, J. Hasan, H.K. Webb, V.K. Truong, G.S. Watson, J.A. Watson, V.A. Baulin, S. Pogodin, J.Y. Wang, M.J. Tobin, Natural bactericidal surfaces: mechanical rupture of Pseudomonas aeruginosa cells by cicada wings, Small 8 (16) (2012) 2489–2494.
[46] Y. Khan, M.J. Yaszemski, A.G. Mikos, C.T. Laurencin, Tissue engineering of bone: material and matrix considerations, Jbjs 90 (Supplement_1) (2008) 36–42.
[47] L. Roseti, V. Parisi, M. Petretta, C. Cavallo, G. Desando, I. Bartolotti, B. Grigolo, Scaffolds for bone tissue engineering: state of the art and new perspectives, Mater. Sci. Eng. C 78 (2017) 1246–1262.